Demand Smoothing in Military Microgrids Through Coordinated Direct Load Control

Spencer C. Shabshab, Peter A. Lindahl, J. Kendall Nowocin, John Donnal, David Blum, Les Norford, and Steven B. Leeb

***Abstract*—In small microgrids and individual branches of a bulk electrical grid, the aggregate electrical load can contain significant and frequent peaks caused by large individual loads. These peaks can reduce overall system efficiencies if generation resources, e.g., diesel generators, are dispatched based on peak demand. This problem is particularly severe in military forward operating base (FOB) microgrids, in which the load profile is dominated by environmental control units (ECUs) that operate under thermostatic control. Leveraging the intrinsic energy storage capabilities associated with large loads such as these ECUs and coordinating their operations across neighboring facilities provides an opportunity to reduce peak demand while maintaining system performance. Using a military FOB microgrid as a use case, this paper presents two direct load control (DLC) algorithms for coordinating ECU operations and reducing peak demand. This coordinated control is demonstrated through simulations and field tests at the U.S. Army's Base Camp Integration Laboratory using novel controller hardware. Both simulation and field tests indicate that the DLC algorithms can reduce peak loads by 25% or more without sacrificing thermal comfort.**

***Index Terms*—Microgrids, smart grids, demand-side management, centralized control, heating systems, temperature control.**

I. Introduction

MILITARY forward operating bases (FOBs) are often located in austere environments lacking access to a bulk power system and thus requiring microgrids for electricity. These FOBs may need to avoid steady wireless communications for security. They distribute power using field distribution boxes that are easily extended to provide networked communications across the base [1]. Delivering fuel to these facilities carries substantial monetary, logistical, and safety costs [2]–[4]. To reduce energy costs, researchers have proposed a variety of solutions including integrating renewable energy resources [5]–[7]. However, due to their intermittent nature and the need for grid reliability for mission critical loads, particularly the electrical components of defense, surveillance, and communication systems, current FOBs still rely heavily on diesel generators for electricity generation [3], [6]. Generators sized for peak conditions will suffer significant inefficiencies when under-loaded [8], [9].

Compared to large-scale transmission networks, where individual loads are "lost" in the aggregate and demand variations occur on a diurnal cycle [10], these FOB microgrids have demand profiles with frequent and significant peaks that dictate generation requirements [11]. These bases have a limited number of "soft" structures, often tents or low-insulation compartments, with high thermal losses and low thermal masses. Deploying thermal storage as a demand response control resource with such structures is an unsolved challenge. The environmental control units (ECUs), i.e., heaters and air conditioners, serving these structures have to cycle frequently under thermostatic control. Periodically, many of the ECUs will be on at the same time. With these ECUs typically representing more than half the FOB's electricity demand [9], [11], [12], this exerts repeated, large temporary peaks on the electrical network. Similarly sized civilian microgrids and sub-branches of the conventional distribution network may also exhibit periodic peaks, though the time between peaks generally increases with the quality of house insulation.

Several approaches applicable to FOBs to match requirements to online generation capacity typically employ a combination of generator dispatch [13], energy storage [14], [15], dynamic energy storage with continuous feedback control, e.g., energy "springs" [16], and load management [17], [18]. Generator dispatch involves dynamically resizing the microgrid's generation capacity by bringing generators on and offline as power requirements change. This is an effective method when the load profile varies slowly enough for generators to dispatch in response.

In microgrids characterized by fast-changing load demands, generators cannot dispatch quickly enough to match demand, and the load profile needs reshaping to improve overall efficiencies. Incorporating *extrinsic* energy storage devices, e.g., batteries, into diesel generator or hybrid-powered microgrids

Manuscript received February 4, 2019; revised May 24, 2019 and August 11, 2019; accepted September 25, 2019. Date of publication October 2, 2019; date of current version April 21, 2020. The work of D. Blum occurred while he was a Building Technology Ph.D. candidate at the Massachusetts Institute of Technology. Paper no. TSG-00189-2019. *(Corresponding author: Peter A. Lindahl.)*

S. C. Shabshab is with the Naval Nuclear Power Training Command, U.S. Navy, Goose Creek, SC 29445 USA.

P. A. Lindahl is with the Electrical Engineering and Computer Science Practice, Exponent Inc., Natick, MA 01760 USA (e-mail: plindahl@exponent.com).

J. K. Nowocin is with CoolCrop, Cambridge, MA 02139 USA.

J. Donnal is with the Weapons and Systems Engineering Department, U.S. Naval Academy, Annapolis, MD 21402 USA.

D. Blum is with the Building Technology and Urban System's Division, Lawrence Berkeley National Laboratory, Berkeley, CA 94720 USA.

L. Norford is with the Department of Architecture, Massachusetts Institute of Technology, Cambridge, MA 02139 USA.

S. B. Leeb is with the Electrical Engineering and Computer Science Department, Massachusetts Institute of Technology, Cambridge, MA 02139 USA.

Color versions of one or more of the figures in this article are available online at http://ieeexplore.ieee.org.

Digital Object Identifier 10.1109/TSG.2019.2945278

can accomplish this, but at the expense of additional capital costs [19], [20]. Alternatively, "deferrable" loads, i.e., those associated with *intrinsic* energy storage capacity [8] such as hot water heaters [21]–[25] and ECUs [18], [26] can be leveraged by direct load control (DLC) schemes to time-shift operation and smooth the aggregate power demand.

DLC approaches leveraging these loads can be categorized as centralized or decentralized, depending on what makes the response decision – the centralized load aggregator or a customer's automated load manager(s) [24], [27], [28]. The benefits of centralized approaches are easier controllability and predictability. As network sizes increase, however, centralized schemes begin to suffer from computational and communication complexities [27]. Decentralized approaches aim to alleviate these issues by distributing these complexities away from a single node. For example, Chen *et al.* present a two-layer control approach [28]. In the upper-layer, load managers interface with the aggregator to learn power consumption targets, and in the lower-level, the manager coordinates individual load operation. For small, islanded microgrids, such as those of the FOB described here, this added layer of complexity is unnecessary as low-computation centralized controllers have been shown to be effective [24].

In [24], the authors present rule-based power management algorithms (PMAs) for reducing microgrid costs and emissions. The DLC algorithms apply to electric water heaters (EWHs) and are used to reduce high cost / high emission power expenditures such as the power delivered from a diesel generator. The same researchers have also investigated demand response of EWHs for frequency and voltage regulation in islanded microgrids via adaptive hill climb and step-by-step control techniques [21], [22].

In addition to EWHs, many researchers have focused on demand response in HVAC systems. For examples, in [29], Chu *et al.* used a least enthalpy estimator-based fuzzy controller to lengthen the off-time of chilled water compressors in buildings while maintaining thermal comfort. Tang *et al.* proposed a multi-optimization control scheme for DLC of air conditioning systems in large commercial buildings [30], and the authors of [31] present an adaptive controller that varies the temperature setpoint of air conditioning systems to comply with permissible power signals from the network operator.

As for previously conducted investigations on demand management at FOBs, Kelly *et al.* [2], [32], [33] designed a power electronic-based energy management system to dispatch multiple generators, batteries, and non-critical loads. This manager was later expanded to accommodate photovoltaics and optimized to minimize energy use [5]. However, in this paradigm, load management was only used to curtail non-critical loads rather than time-shift individual loads. More recently, Sprague [9] developed a simulation model of a 45-person Marine Corps FOB containing several shelters, multiple generators of varying capacity, and a battery-based energy storage system. The author then used a mixed-integer linear programming (MILP) approach to schedule ECU runtimes in an effort to optimize generator dispatch. Olabode [34] furthered this research by analyzing the efficiency improvements of such an optimization scheme with the addition of renewables and the presence of uncertainty in demand scheduling. The vast majority of these load management schemes designed to time-shift loads are concerned with smoothing demand peaks on a diurnal scale. Those that are concerned with intra-hour peak balancing [9], [18], [34], require dynamic models for forecast-and-update optimization or to iteratively find an optimal solution. This can be computationally burdensome.

The FOB infrastructure provides a natural means and preference for centralized control. Power is distributed through quick-connect "Distribution Manager" boxes in the field [1], a portable infrastructure that is easily modified to include distributed, wired communication while maintaining communication security unavailable from wireless schemes. This paper presents new load management approaches for an Army FOB based on the Army's Force Provider (FP) module [1]. Central to this management scheme are two novel, low-computation control algorithms for coordinating ECU operation and reducing peak demand while simultaneously preserving occupant comfort. These algorithms do not require dynamic thermal models, with one algorithm using a steady-state model and the other requiring no model at all. Unlike the many other approaches reviewed above, the approach here does not require a large thermal mass, added energy storage, or high-bandwidth power electronic controls. In fact, the peak demand control schemes presented here require no new power electronic modifications and can work with the existing drive hardware found in the FOB and most other ECUs. These algorithms can serve as the basis for improving energy efficiency and reducing fuel use at the FOB.

Of the DLC schemes concerned with long-term demand smoothing, the rule-based algorithm of [24] applied to electric water heaters contains some similarities to those we present here. First, the control scheme explicitly limits the maximum number of simultaneously operating heaters so as to limit peak loads. We similarly define such a constraint on the number of operating ECUs in the algorithms presented here. Further, the rule-based algorithm also relies on a protocol for prioritizing water heater operation based on their water temperatures, while our algorithms similarly prioritize ECU operation based on the temperatures of their corresponding tent compartments. However, in contrast to our algorithms, the rule-based algorithm of [24] requires a dynamic model of the water heaters and other major components in the microgrid. Further, the operating rules of the algorithm are concerned with simply limiting the power provided by the grid's batteries and diesel generator, whereas the operating rules of the our algorithms are designed to maximize the loading of the minimum number of generators required for meeting load demand.

While not required for the algorithms, this paper develops combined dynamic thermal models for the ECUs and their tent structures based on measured data collected at the U.S. Army's Base Camp Integration Laboratory (BCIL) at Ft. Devens, MA. For testing and demonstrating these algorithms, we develop a fully modular object-oriented FOB simulation environment in MATLAB consisting of these thermal models as well as fuel-usage models for the camp's generators. This paper also presents communication and coordination hardware that

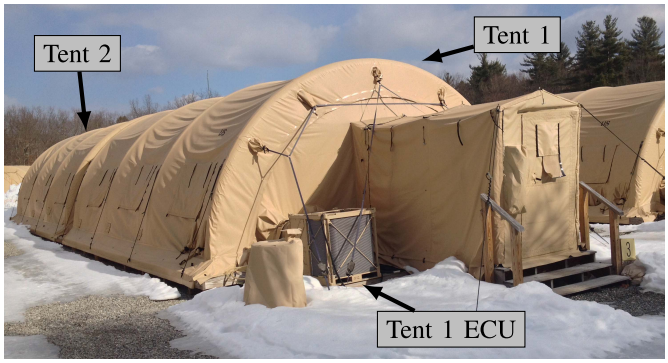

Fig. 1. The majority of FOB structures are billeting complexes (two adjoined tents each with an ECU).

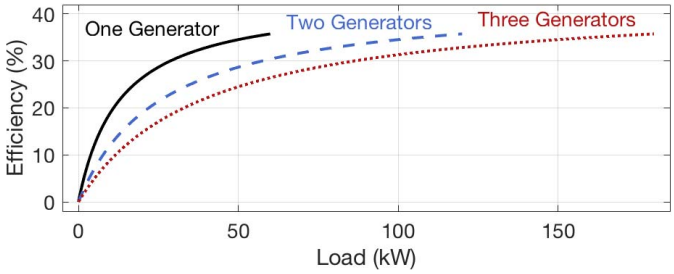

Fig. 2. Estimated efficiency curves for paralleled 60kW diesel generators.

retrofits inside Army ECUs facilitating coordinated network control. Finally, we present field test results achieved at the BCIL that demonstrate the coordinated ECU control and peak-load reduction in a real-world environment.

II. The Army's Forward Operating Base

The Army's Force Provider (FP) [1] is designed for rapid deployment and operation in both hot and cold environments. A single FP "module" contains multiple billeting tents (Fig. 1), generators, ECUs, showers, latrines, kitchen services, and their associated equipment. Each module supports between 50 and 150 persons and can be dispatched individually or grouped to form larger FOBs.

A. Electricity Generation

FP modules generate electricity from a bank of identical 60kW synchronous diesel generators. In steady-state, diesel generators are well-modeled with fuel consumption rates ($\dot{m}$) following a linear relationship with load [8], i.e.,

$$\dot{m}(P_{load}) = \dot{m}_0 + \dot{m}_1 \frac{P_{load}}{P_{g,rated}} \tag{1}$$

Here, $\dot{m}_0$ is the no-load rate, while $\dot{m}_1$ is the slope at which the rate varies with normalized load ($P_{load}/P_{g,rated}$). $P_{g,rated}$ is the rated power of a single generator, and P_{load} is the load supplied by the generator.

Under the default FP module configuration, these generators operate in "stand-alone" mode, each powering a subset of a module's assets. While simple to set up, this configuration leads to significant inefficiencies in fuel use as every dispatched generator remains online even during times of light aggregate electricity demand. To improve the generator efficiency, the FP can be set up as a microgrid with the generators colocated and connected in a ring-bus fashion. Electricity is then distributed radially from this ring-bus to the loads via distribution boxes. In this configuration, the generators can be paired with control equipment for paralleling generators so they can dispatch in response to load demand generator-dispatch control). Specifically, with N generators online, this controller spins up an additional generator if the total load exceeds 80% of the N generators' capacity for longer than 10 seconds, and spins down a generator if the total load decreases below 60% of the capacity of $N-1$ generators for longer than five minutes.

When paralleled, each dispatched generator nominally shares the load equally. This is a reasonable assumption as the generators are colocated and connected with short cables that present smaller impedances than those of the longer lines connecting the generators to their loads. Further, each distribution branch provides power to a subset of the camp, e.g., a pair of billeting tents. Under this configuration, as long as the camp's non-ECU loads are distributed so as not to overload any single distribution branch, the network does not present operational constraints (as discussed in [35], [36]) that would limit the ability to enact either DLC or the generator-dispatch control. Equation (1) can therefore be expanded to describe the fuel consumption rate of multiple paralleled generators as,

$$\dot{m}(P_{load}, N) = N\dot{m}_o + \dot{m}_1 \frac{P_{load}}{P_{g,rated}} \tag{2}$$

where each generator provides a $\frac{1}{N}$ fraction of the total load, P_{load}. The efficiency of the N generators is,

$$\eta(P_{load}, N) = \frac{P_{load}}{\dot{m}(P_{load}, N)LHV} \tag{3}$$

where LHV is the lower heating value of the generator fuel (33 MJ/L for JP-8 fuel). Fig. 2 shows the estimated operating efficiencies derived from fuel rate data provided in [37] for simultaneously operating generators as a function of total load. For these curves, $\dot{m}_0$ and $\dot{m}_1$ were estimated as 3.2 L/hr (0.85 gal/hr) and 15 L/hr (4.0 gal/hr), respectively. Thus, operating with the minimum number of generators required for the total load can result in significant efficiency gains.

B. Dominant Loads: Billeting Tents With ECUs

The dominant electrical loads at an Army FOB are the distributed ECUs [9], [12], which maintain desirable temperatures in a FOB's various structures. For FP modules, the majority of these structures are billeting tents typically adjoined back-to-back in pairs to form a complex as shown in Fig. 1.

The dynamic thermal performance of these complexes can be described using lumped elements as shown in Fig. 3. Here, the thermal capacitances, $C_{t,i}$, represent the two tents ($i = 1$ and $i = 2$), with internal temperatures, $T_{t,i}$. The tents interact with the outside environment, represented here as a thermal reservoir, T_e, via thermal impedances, $R_{te,i}$. The tents also absorb heat sourced from the sun ($P_{s,i}$) and exchange heat with each other through convective heat flow (R_{tt}). Each tent's ECU provides heat ($P_{h,i}$) to its tent. These ECU heaters normally

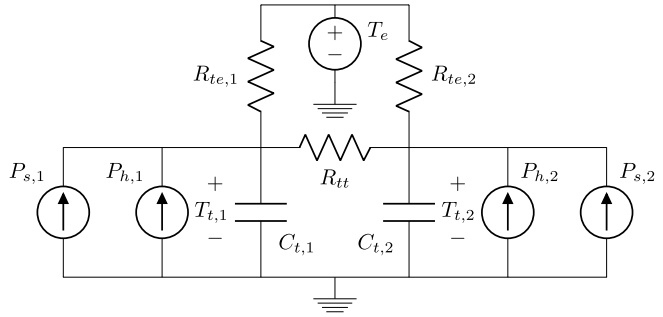

Fig. 3. Billeting complex model. Subscripts '1' refer to tent Section I, subscripts '2' refer to tent Section II.

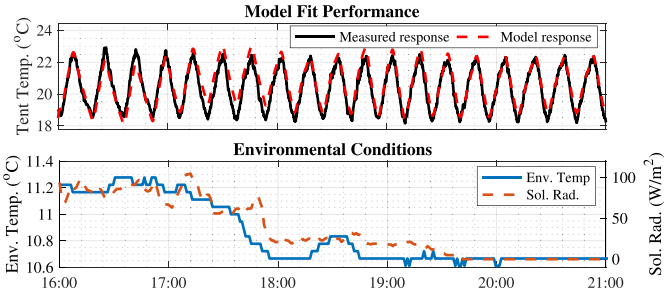

Fig. 4. Representative example of model fit performance for a single tent section.

TABLE I
BILLETING COMPLEX MODEL PARAMETERS

	$C_{t,i}$ (kJ/K)	$R_{te,i}$ (K/kW)	R_{tt} (K/kW)	$k_{s,i}$ (W/m^2)	$\tau_{h,i}$ (s)
Max	444	2.27	4.0	22.1	91
Min	332	1.76	2.3	9.8	43.5

operate under thermostatic bang-bang control with rated output power $P_{h,rated} = 9$kW when on and 0kW when off. Due to latencies in propagating hot air from the ECU into the tent sections, the rate of heat supplied from the ECU to the tent follows a first order differential equation,

$$\dot{P}_{h,i}(t) = \frac{1}{\tau_{h,i}}\big(P_{h,rated} - P_{h,i}(t)\big). \tag{4}$$

Here, $\tau_{h,i}$ is a time constant related to the time required to move this heated air.

The rate of solar heat absorption in each tent is modeled as,

$$P_{s,i}(t) = k_{s,i}P_{sol}(t). \tag{5}$$

where $P_{sol}(t)$ is the global horizontal irradiance (GHI) measured at the base's weather station, and $k_{s,i}$ is a scaling constant accounting for the location and orientation of each tent section relative to the sun.

The BCIL at Fort Devens, MA contains an archetypal FOB comprised of two FP modules. Using data collected at the BCIL, we fit the billeting complex models of Fig. 3 and (4), (5) to the temperature performance of four billeting complexes using the **greyest()** command in MATLAB. Table I shows the extent of the parameter value fits, while Fig. 4 provides a representative comparison of the resulting model temperature output to measured data for one of the billeting tents over a six hour window.

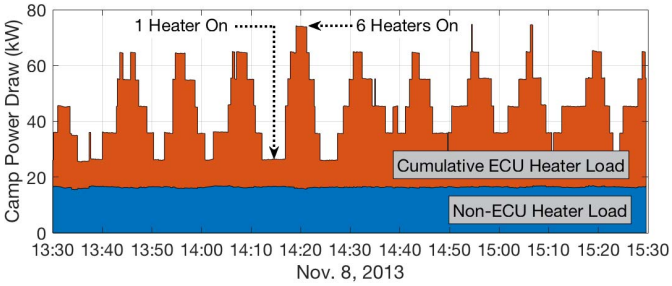

Fig. 5. ECUs providing climate control to FOB structures can dominate the aggregate power demand of the FOB and cause large peaks in power draw when their on/off times overlap.

TABLE II
ENERGY SAVINGS OPPORTUNITY

Electrical Configuration	Avg. Gen. Dispatch	Avg. Gen. Capacity	Fuel Use (L/hr)	Electrical Efficiency
Minimum stand-alone	2	38%	35.3	27%
Generator dispatch	1.86	42%	34.4	28%
Ideal ECU coordination	1	75%	28.9	33%

III. EFFICIENCY BENEFITS OF COORDINATED CONTROL

The low thermal capacitances and high thermal losses of the complexes cause the ECUs to cycle frequently. This results in significant and recurrent peaks in the camp's aggregate power load as ECU operations overlap in time. Fig. 5, showing a two hour window of electricity consumption measured at the BCIL during a cold weather training exercise involving 90 soldiers [12], illustrates this phenomenon. Using Nonintrusive Load Monitoring (NILM) transient identification techniques [38], we disaggregated the energy delivered to the ECU heaters from the bulk electrical measurements. The blue (lower) area in Fig. 5 shows the total non-ECU heater load for one of the FP modules. The orange (upper) area shows the cumulative ECU heater load. During this time period, the Non-ECU heater load was stable but the cumulative ECU heater load varied significantly and often as the number of simultaneously operating ECUs varied.

At the BCIL, each module's electrical network is by default configured as a microgrid powered directly from the local utility rather than from the camp's generators to save on operational costs and reduce generator wear. However, from (2) we can estimate the energy expenditures that the module would have incurred if powered from the generators in stand-alone mode or operating under dispatch control (Table II).

Taking the two hour window of Fig. 5 in isolation, *at minimum* two stand-alone generators would have been required as peak demand eclipsed the capacity rating of a single generator. Each of these two generators would have only operated at 38% capacity on average for an effective electrical generation efficiency of 27%. Configuring the module as a microgrid with generator dispatch control would have only modestly improved efficiencies to 28%. This is due to the frequent peaks in the electrical demand and the slow spin-down response of the generator control, resulting in a second generator dispatched for over 100 minutes of the two hour window. However, if

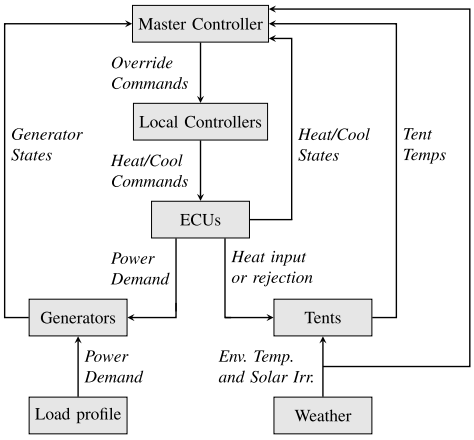

Fig. 6. Simulation environment module and information flow schematic.

the ECU heaters were coordinated to reduce their maximum simultaneous operations, the peak load would decrease towards the average load of 44kW. In this situation, only one generator would need to operate, resulting in an 18% reduction in fuel use from the *best-case* stand-alone generator paradigm.

IV. Microgrid Simulation Environment

Fig. 6 provides the module and information flow schematic for a MATLAB-based object-oriented simulation environment that enables exploration of coordinated control techniques and their costs and benefits. The environment is a conglomerate of various modules, each containing its own programmable decision logic and/or dynamics. The ECUs and tents modules combine to enact the billeting complex models of Fig. 3 and (4), (5), while the generators module contains the steady-state generator models of (2) and (3) along with the generator dispatch rules. The load profile and weather modules allow a user to incorporate arbitrary non-ECU electrical load profiles and weather profiles, respectively, including profiles derived from historical data. Finally, the master controller (MC) and local controller (LC) modules contain the programming to realize coordinated control algorithms (or other control objectives).

In Fig. 6, the information passed between modules is depicted with arrows indicating the information flow direction. The MC, which acts as the "brain" for any centralized control scheme, receives information on the generator and ECU states, the tent temperatures, and weather information, any or all of which can be used for decision making. The MC passes high-level operation commands (listed here as override commands as the LCs override the internal programming logic of the ECUs) to the LCs, which in turn dictate the heating and/or cooling modes and timings of the ECUs. The generators receive load information from the individual ECUs and load profile module.

The modules are defined by and exist as properties of a FOB object, where the user controls the duration and timestep of the simulation. This FOB object importantly gives the user the ability to dictate the FOB composition in terms of the number of generators, tents/ECUs, and their model parameters. In this way, the environment allows for rapid investigations into a range of control and load configuration scenarios, and how the various components of a FOB's electrical system interact. Further information on this simulation environment can be found in [11].

V. Load Spreading Control Algorithms

Two centralized control schemes are presented here as alternatives to the thermostatic regime, and their performance is demonstrated using the simulation environment of Section IV. Each controls the states of distributed ECUs with the dual objectives of attaining acceptable temperature performance and limiting the aggregate peak ECU load. The presentation and evaluation of these algorithms focuses on ECU operation in its heating mode (with the assumption that the environmental temperature is lower than the desired temperature of the tent compartments).

These algorithms are broadly applicable to resistive-heating systems as well as cooling systems that operate under various forms of on-off or pulse-width modulated (PWM) control, though this requires additional considerations for the heat pump's dynamics and nonlinear performance. The FP-module ECUs are in this group as they feature a form of PWM control where their scroll-compressors can be engaged/disengaged to rapidly vary the unit's cooling performance and power consumption. Other cooling systems, e.g., chillers featuring variable speed drive (VSD) motors [39], improve overall efficiency by adjusting its operational capacity to match cooling needs [40].

The two control schemes, "band-seeking" and "average-seeking" give precedence to a peak load constraint, expressed here in terms of a maximum number of simultaneously operating ECUs. The algorithms differ primarily in how they determine device cycle times, and in how they operate when the peak load constraint precludes achieving temperature setpoints. Also of note, the band-seeking algorithm does not require a model of the thermal system being controlled, while the average-seeking algorithm does.

A. Band-Seeking Control

The band-seeking centralized ECU control algorithm attempts to control distributed ECUs such that each tent section temperature $T_{t,i}$ remains within ΔT degrees of the tent section setpoint $T_{s,i}$, subject to the peak load constraint. That is,

$$\left|T_{s,i} - T_{t,i}\right| \leq \Delta T \quad \text{for all } i \tag{6}$$

$$\sum_{i=1}^{N} \delta_i \leq N_{max} \tag{7}$$

where δ_i is equal to 0 if the i^{th} heater is off and equal to 1 if it is on, and N_{max} is the maximum number of heaters permitted to operate simultaneously. Individual compartments are permitted to have different temperature setpoints but ΔT is equal among the tents.

Algorithm 1 Band-Seeking ECU Control Logic

Input: Temperature setpoints $\mathbf{T_s}$, compartment temperatures $\mathbf{T_t}$, temperature bandwidth ΔT.
$\mathbf{e} = \mathbf{T_t} - \mathbf{T_s}$ {compute temperature deficits}
for all tents with ECUs on **do**
  i = tent #
  if $e_i > \Delta T$ **then**
    turn ECU i OFF
  end if
end for
for all tents with ECUs OFF (in ascending order of e_i) **do**
  i = tent #
  if $e_i < -\Delta T$ **then**
    if # ECUs on $< N_{max}$ **then**
      turn ECU i ON
    else
      k = tent # with maximum e_k of all tents with ECUs ON
      if $e_k > e_i + 1.5\Delta T$ **then**
        turn ECU k OFF
        turn ECU i ON
      end if
    end if
  end if
end for

Under band-seeking control, the MC turns off a heater when its tent's temperature rises above the allowed temperature range, and turns it on when this temperature falls below its range, provided that the number of heaters operating does not already equal N_{max}. If the compartment temperature is below range and the number of heaters operating is at its limit, the MC searches for a tent with its heater on that is closer to the top of its temperature band (by $1.5 \times \Delta T$). If the MC finds such a tent, it turns that tent section's heater off and turns on the heater of the worse-off tent. This control logic is described by Algorithm 1. Here, bolded variables indicate arrays, e.g., $\mathbf{T_t} = [T_{t,1}, \ldots, T_{t,N}]$ is the array of all tent temperatures. Fig. 7 shows the simulated control of a FOB with $N = 8$ tents each with $T_{s,i} = 20°\text{C}$ and $\Delta T = 2°\text{C}$ under various values for N_{max}. The simulated environmental conditions (T_e and P_{sol}) are those shown in Fig. 4.

1) Peak Load Unconstrained: Under no peak load constraint ($N_{max} = \infty$), the band-seeking algorithm is identical to the thermostatic regime (Fig. 7(a)). Heaters operate until the controlled compartment temperature rises to the upper temperature bound and then turn off until the temperature falls to the lower temperature bound.

2) Peak Load Constrained, ECUs Can Achieve Setpoints: When N_{max} does restrict simultaneous heater operations, the MC attempts to meet all temperature setpoints in accordance with Algorithm 1. In Fig. 7(b), the band-seeking algorithm enforces a maximum of five simultaneous heater operations (down 29% from seven in the unconstrained steady-state perform), which restricts the heater operations but not to the point that temperatures drop outside their target bands.

3) Peak Load Constrained, ECUs Cannot Achieve Setpoints: If N_{max} constrains heater operations to a point that they cannot achieve their temperature setpoints, the MC enforces all tent section temperatures to fall equal amounts below their temperature setpoints as shown in Fig. 7(c). The control accomplishes this despite the differing thermal characteristics (Table I) in the various tent sections. Under these conditions, the algorithm effectively spreads load shedding across all tents.

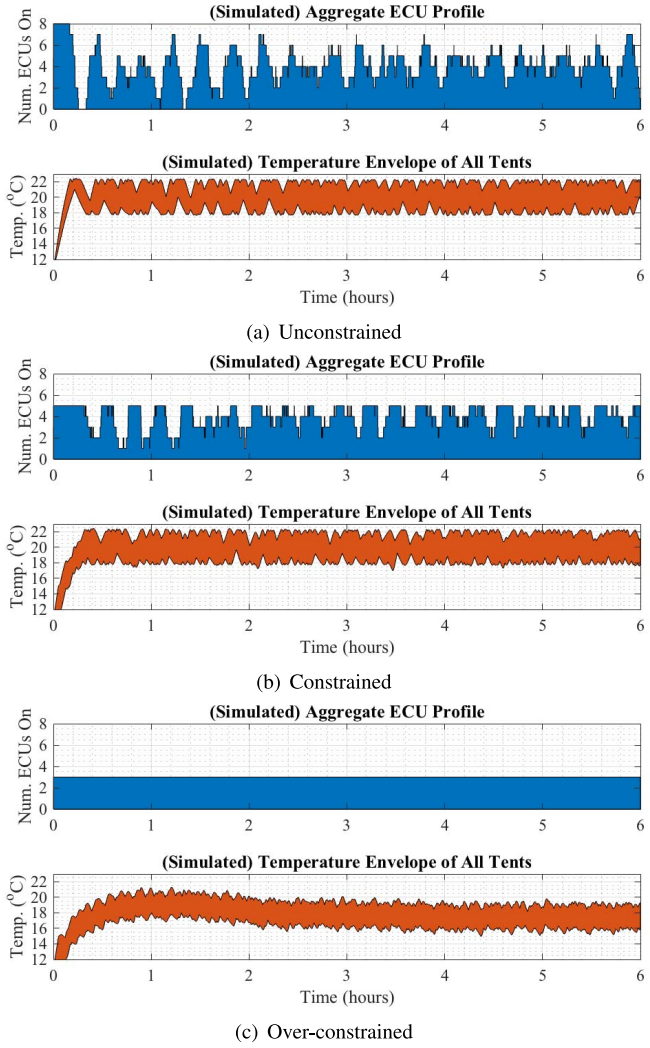

(a) Unconstrained

(b) Constrained

(c) Over-constrained

Fig. 7. Operation of the band-seeking algorithm, (a) under no peak load constraint, (b) under the constraint of $N_{max} = 5$, which restricts heater operations but not to the extent that temperatures fall outside the target band of 18 - 22°C, and (c) under the constraint of $N_{max} = 3$, which does restrict heaters to the point that temperatures dip outside the target band.

B. Average-Seeking Control

The average-seeking centralized ECU control algorithm attempts to schedule distributed ECUs such that each tent's temperature averaged over each schedule period equals its respective temperature setpoint. The lengths of these schedule periods, t_{sch}, should be set short enough to protect against wide swings in temperatures, but not so short to cause excessive switching of equipment contactors. That is, the maximum period time is related to the thermal time-constants of the tents, the controller temperature limits, and the range of temperatures expected at the FOB, while the minimum period limit depends on the cycle-life of the contactors used in the controller hardware. Like the band-seeking algorithm, the average-seeking algorithm is subject to the peak load constraint of (7).

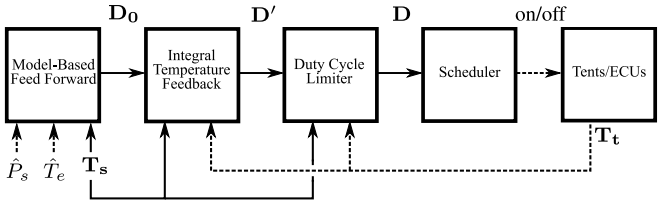

Fig. 8. Block diagram of the average-seeking centralized control regime. Solid lines denote signals that update only when a new schedule is created, and dashed lines indicate signals that are updated every time step.

Fig. 8 depicts the average-seeking control flow, which begins with a feed-forward stage that provides an estimate of the duty cycle with which each heater must operate over the n^{th} scheduling period to maintain the desired average temperature setpoint. These estimates are based on steady-state models of the billeting complexes derived from the dynamic model of Fig. 3 with the capacitances replaced by open-circuits and $T_{s,i}$ set to the desired values for the schedule period. Using weather forecast estimates, i.e., $\hat{T}_e$ and $\hat{P}_{sol}$, the latter of which provides estimates of $P_{s,i}$ via (5), the billeting complex model can be solved for $P_{h,i}$. From these solutions, the feed-forward duty cycle estimate for tent i during the n^{th} schedule period is,

$$D_{0,i}[n] = \frac{P_{h,i}(nt_{sch})}{P_{h,rated}}. \tag{8}$$

Here, nt_{sch} is the time when the n_{th} schedule period begins, and the $[\,\cdot\,]$ notation indicates that n and $D_{0,i}$ are discrete variables.

The integral temperature feedback module continuously integrates each tent's temperature error as,

$$D_{int,i}(t) = k_{int}\int_0^t T_{t,i}(t) - T_{s,i}(t)dt, \tag{9}$$

subject to the anti-windup constraints,

$$D_{int,min} \le D_{int,i}(t) \le D_{int,max}. \tag{10}$$

In (9), k_{int} is the integral gain. $D_{int,i}(t)$ is then added to the feed-forward duty cycle estimate at the beginning of each schedule period, n, and prior to submission to the duty cycle limiter module,

$$D_i'[n] = D_{o,i}[n] + D_{int,i}(nt_{sch}). \tag{11}$$

The duty cycle limiter imposes the constraint of (7) in a way that proportionally weights the individual ECU duty cycles by the extent their average temperature error over the previous schedule period exceeds the average error of all the tents. The initial (n =0) maximum duty cycle constraints are equal among ECUs such that,

$$D_{max,i}[0] = \frac{N_{max}[0]}{N}. \tag{12}$$

As the ECUs operate, the maximum duty cycles update at each new schedule period based on the average error of the previous schedule period, i.e.,

$$\bar{e}_i[n] = \frac{1}{t_{sch}}\int_{(n-1)t_{sch}}^{nt_{sch}} \big(T_{s,i}(t) - T_{t,i}(t)\big)dt \tag{13}$$

Algorithm 2 ECU Scheduling Logic for the Average-Seeking Control Regime

Input: Duty cycle requests **D**, number of time segments N_{seg}.
  $\mathbf{s} = \text{round}(N_{seg}\mathbf{D})$ {calculate # of segments each ECU is ON}
  assign ECU 1 to time segments 1 through s_1
  for $i = 2$ through N {step through remaining ECUs} **do**
    x = time segment after last allocated
    if $x + s_i - 1 \le N_{seg}$ **then**
      assign ECU i to time segments x through $x + s_i - 1$
    else
      assign ECU i to time segments x through N_{seg}
      assign ECU i to time segments 1 through $s_i - N_{seg} + x - 1$
    end if
  end for

$$D_{max,i}[n+1] = D_{max,i}[n] + k_{max}\left(\bar{e}_i[n] - \frac{\sum_{k=1}^{N}\bar{e}_k[n]}{N}\right) \tag{14}$$

with, k_{max} a scalar tuning parameter for updating $D_{max,i}$. The duty cycle, $D_i[n]$ then submitted to the scheduling algorithm equals $D_i'[n]$ if $D_i'[n] < D_{max,i}[n]$, and $D_{max,i}[n]$ if it is not. This limitation distributes the cumulative available heater operation time among the ECUs so that all tent temperatures fall equal amounts below their setpoints if the peak load constraint prevents all compartments from reaching their average temperature setpoints.

The final stage of the average-seeking control for the MC is the ECU on/off time scheduler. Here, the MC segments each schedule period into N_{seg} equal-length time steps. Using the scheduling algorithm detailed in Algorithm 2, the MC assigns ECU operation to sections of time segments and communicates on/off commands to each LC accordingly. The MC renews the schedule at the beginning of each schedule period.

Fig. 9 shows the simulated control of an $N = 8$ tent FOB with $T_{s,i} = 20°\text{C}$ under the same environmental conditions as Fig. 7 and with varying N_{max} constraints. For both simulations, t_{sch} was set to 12 mins.

1) Peak Load Unconstrained, ECUs Can Achieve Setpoints: Under average-seeking control, Algorithm 2 minimizes the maximum number of heaters active during any time segment. Thus, if $D_i[n]$ is unconstrained by (14), then N_{max} does not affect the control scheme's performance and the tent temperatures meet their setpoints. Fig. 9(a) shows the performance of the algorithm when $N_{max} = 5$ (performance would be identical for $N_{max} > 5$), which is equal to the minimum number of simultaneous heater operations required to maintain tent temperatures (also down 29% from the peaks number of ECUs under the unconstrained band-seeking control equivalent to thermostatic control).

2) Peak Load Constrained, ECUs Cannot Achieve Setpoints: If N_{max} is less than 5, the constraint of (14) limits the peak load and the heaters cannot achieve their temperature setpoints. Fig. 9(b) depicts the scenario where $N_{max} = 3$. In this case, the number of simultaneous heater runs "rails" at 3, and the constraints of (14) ensures that all tent sections share the resulting load shedding, with temperatures falling equal amounts below their temperature setpoints (approximately 2°C below the setpoint of 20°C).

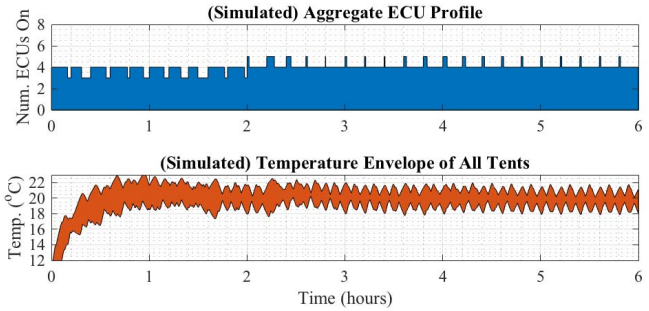

(a) Under-constrained

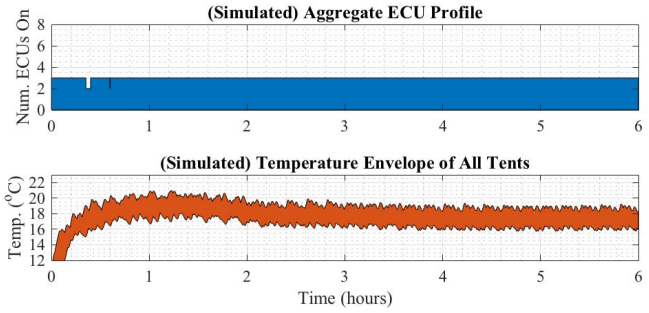

(b) Over-constrained

Fig. 9. Operation of the average-seeking algorithm, (a) when the peak load constraint $N_{max} = 5$ does not affect the tents' temperature performance, and (b) when the constraint $N_{max} = 3$ does restrict heaters to the point that the temperature dips away from the setpoint of 20°C.

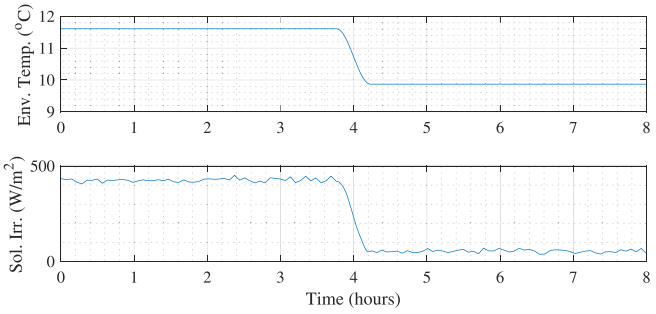

Fig. 10. Simulated sudden unforecasted change in weather where the environmental temperature drops 4°C and the average solar irradiance drops 100W/m^2 over a 15 minute period.

C. Algorithm Responses to Forecast Uncertainty

The simulated FOB's DLC performance under each of the two algorithms described above was also evaluated in response to a series of several unforecasted simulated step changes in weather. The performance of the algorithms is not predicated on a dynamic model of temperature in the tents. Step changes are, therefore, an effective way to illustrate the performance of the algorithms, as these changes expose the most dramatic variabilities likely to be seen by the FOB. An example step change is provided in Fig. 10, where the temperature and the solar irradiance drop approximately 2°C and 400W/m^2, respectively, over a period of 20 minutes.

Fig. 11 shows the response of the simulated FOB while under band-seeking control. Because this algorithm is effectively a modification of thermostatic control and it does not

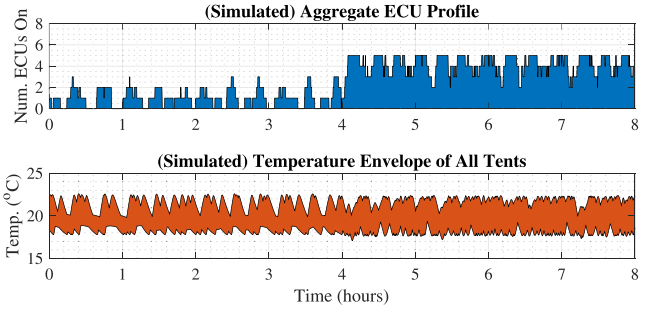

Fig. 11. Simulated response of the band-seeking algorithm to the unforecasted weather change.

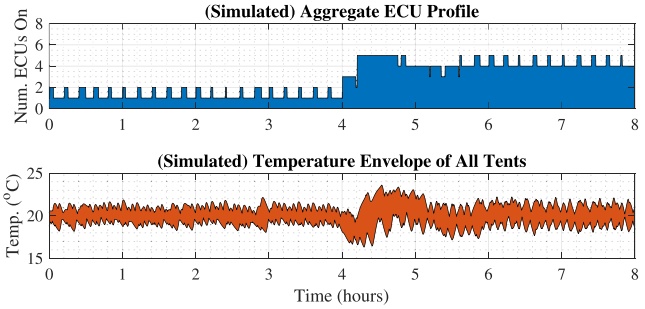

Fig. 12. Simulated response of the average-seeking algorithm to the unforecasted weather change.

rely on a model, the MC is able to dictate heater operations immediately upon individual tent temperatures reaching the lower limit. During the drop in weather conditions, the average number of heaters simultaneously operating ramps up until the temperature and solar irradiance stabilizes.

Fig. 12 shows the response under average-seeking control. Unlike the band-seeking control approach, this control uses the camp model with forecasted weather data as input in a feed-forward control stage. The unforecasted change in weather then creates an error in the feed-forward duty cycle estimate that needs to be corrected by the feedback stage. This results in the disturbance in the tent temperatures, where the minimum tent temperature falls to 16.3°C and the maximum tent temperature reaches 23.6°C before converging back to the desired levels. The reader is reminded however that these temperature plots represent the aggregate temperature envelope for the entire FOB. During this simulation, no individual tent temperature exceeds or falls below the desired temperature range for longer than 10 minutes.

VI. Field Testing Networked ECUs

To facilitate field testing of coordinated environmental control, we developed a network-based control scheme consisting of a master controller (MC), a local area network (LAN), and eight local controllers (LCs), and installed the system at one of the FP modules at the BCIL. The MC, a laptop personal computer, receives feedback data, e.g., tent temperature, from each LC and sends control signals, e.g., heater on or off, back to each LC via the LAN. The MC control logic and communication programming are implemented in MATLAB. The

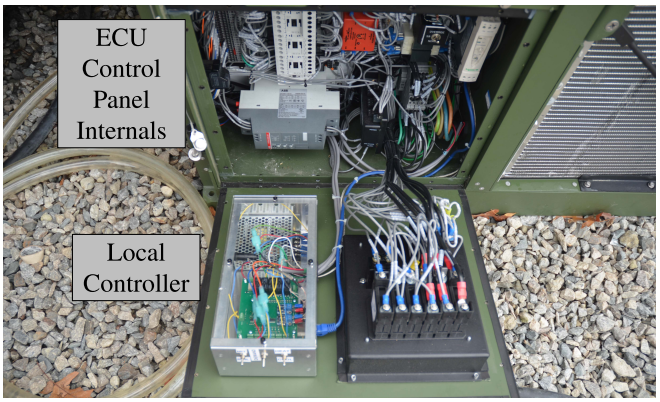

Fig. 13. A local controller retrofit in an ECU control panel.

LCs are Raspberry Pi-based devices that fit inside the ECU's electronics panel and retrofit to its control circuitry as shown in Fig. 13.

A. Local Control of ECU Operation

Each LC exchanges information with the MC via Modbus TCP. Using six mode control relays (MCRs) and two digital-analog converters (DACs), each LC bypasses the internal controls of the ECU, allowing networked control of each ECU's mode (**Heat**, **Cool**, **Vent**, or **Off**) and temperature setpoint. Two thermocouples sense the ECU's outlet and return air temperatures, and eight analog-digital converter (ADC) channels on each LC allow monitoring of ECU performance, e.g., temperatures, fault signals, etc.

While in **Heat** mode, the ECU normally controls its resistive heater thermostatically (with a temperature window of approximately $\pm$ 2°C) based on its temperature setpoint and the return air temperature. The heater energizes via a contactor actuated by a low-power relay. The LC bypasses the ECU's heater actuation circuits via an MCR to control the relay directly. While not discussed in this paper in terms of networked control, the LC can actuate and control the ECU in **Cool** mode as well, using MCRs to engage/disengage the ECU's scroll compressor.

In all modes except for **Off**, the ECU's compartment ventilation fan draws air into the ECU via the return duct. This air then passes over the evaporator coils or resistive heater if in **Cool** or **Heat** mode, respectively, and circulates back into the tent via the outlet duct. When in **Vent** mode, neither the evaporator coils nor resistive heater are at temperature and so the result is simply recirculation of the air. In **Cool** mode, an additional fan passes air over the condenser coils to expel heat to the environment. The LC does not control the functions of the ventilation fan nor the condenser fan, instead allowing the ECU to dictate control based on the ECU's mode (which is controlled by the LC).

B. Field Test Proof-of-Concept

A field test performed at the BCIL demonstrated networked ECU control (Fig. 14). During these test, two billeting complexes comprising four tents were left under traditional ECU

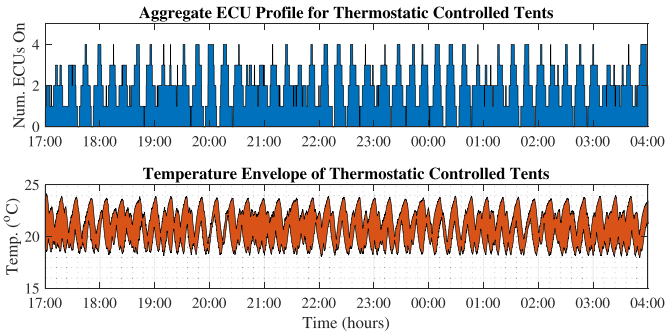

(a) Traditional Thermostatic Control

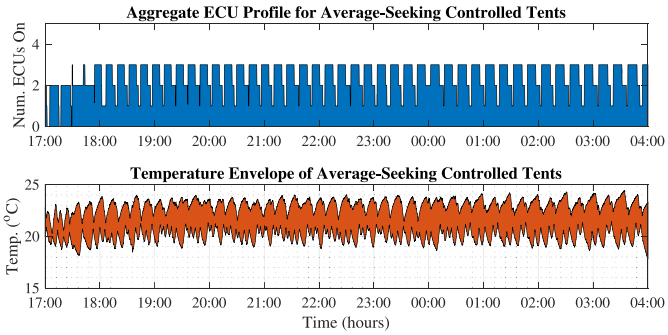

(b) Average-Seeking Control

Fig. 14. Comparison of the ECU operation and temperature performance of four tent complexes at the BCIL with (a) two complexes under traditional thermostatic control, and (b) two complexes under an average-seeking control.

control (Fig. 14(a)), while two other billeting complexes were placed under centralized control (Fig. 14(b)), allowing direct comparisons in performance. The outdoor temperature during this test averaged 10.5°C. The centralized ECU control algorithm applied in this test was a preliminary version of the average-seeking control regime with $t_{sch} = 14$ mins. Notably, this preliminary control used a slightly different scheduling algorithm than the one described in Algorithm 2. This different algorithm minimizes the maximum simultaneously operating heaters, but does not guarantee maximum flatness in the aggregate demand as Algorithm 2 does. This is evident in the top plot of Fig. 14(b) as the number of simultaneously operating heaters fluctuated between 1 and 3. Still, the test serves as hardware validation and experimental proof-of-concept to show the peak-shaving potential of centralized ECU control. Comparing the two figures, the temperature performance of all centralized controlled tents varies between approximately 19 and 24°C, a similar range for the traditionally controlled tents, but the number of simultaneously operating ECUs was limited to 3 instead of fluctuating between 0 and 4. Thus, the control scheme reduces the peak load by 25% while still maintaining tent temperatures.

VII. Discussion & Conclusion

This paper presents novel control algorithms for coordinating loads across neighboring facilities in order to reduce the aggregate peak demand presented on a military FOB microgrid. Neither algorithm requires significant computation power, and unlike model predictive control techniques, the

band-seeking algorithm does not require thermal models for executing its control scheme. When simulated in the presence of a sudden unforecasted change in weather, the band-seeking algorithm performed better at maintaining compartment temperatures with no deviation from the target range. While the average-seeking algorithm allowed tent temperature deviations outside the range, these deviations could be improved or eliminated with better tent models and better tuning of the feedback controller. Additionally, a potential benefit of the average-seeking algorithm is that the model-based feedforward controller lends itself to use in predictive control methods [41].

The paper also presents proof-of-concept field tests demonstrating peak demand reduction while maintaining occupant comfort. On their own, these control algorithms effectively reduce peak demand first through coordinated control and then through distributed load shedding if constrained by a maximum load setpoint.

The tent complexes comprising the Army FOB are "quick-to-erect" structures with marginal insulation, and their low thermal capacity and high thermal losses mean the thermal time constants of these structures are short (on the order of minutes). Structures with such low-quality thermal storage characteristics are typically not considered for such demand-response applications. However, under the algorithms presented here, these assets prove sufficient for shifting load operations enough to smooth the aggregate demand and improve the operational efficiencies of the camp's generators.

These algorithms could also be adapted for other applications. For example, they could be adapted for other islanded microgrids and small localizations of conventional distribution networks. One particularly interesting application would be to group utility customers participating in DLC programs into ensembles. These participants could then have their air conditioners coordinate, effectively "throttling" their units during peak times rather than having them fully shut off. These capabilities could also help limit the rebound effect during payback periods [30].

ACKNOWLEDGMENT

The authors thank the staff at the U.S. Army's Base Camp Integration Laboratory (BCIL), Fort Devens, MA, USA for their technical advice and access to their facilities. The authors also thank the Grainger Foundation and Exelon for their financial and technical support.

REFERENCES

[1] "Force provider operations," Dept. Army, Washington, DC, USA, Rep. ATP 4-45 (FM 4-20.07), 2014.
[2] R. L. Kelly, G. Oriti, and A. L. Julian, "Reducing fuel consumption in a forward operating base using an energy management system," in *Proc. IEEE Energy Convers. Congr. Expo.*, Sep. 2013, pp. 1330–1336.
[3] "Sustainable forward operating bases," Noblis, Reston, VA, USA, Rep. ADA571503, 2010.
[4] D. Eady, S. Siegel, R. Bell, and S. Dicke, "Sustain the mission project: Casualty factors for fuel and water resupply convoys," Army Environ. Policy Inst., Arlington, VA, USA, Rep. ADB356341, 2009.
[5] N. Anglani, G. Oriti, and M. Colombini, "Optimized energy management system to reduce fuel consumption in remote military microgrids," *IEEE Trans. Ind. Appl.*, vol. 53, no. 6, pp. 5777–5785, Nov./Dec. 2017.
[6] X. Qiu, T. Nguyen, M. L. Crow, A. C. Elmore, and B. McMillin, "Computer models for microgrid applications," in *Proc. IEEE Power Energy Soc. Gen. Meeting*, Jul. 2011, pp. 1–8.
[7] M. S. Scioletti, A. M. Newman, J. K. Goodman, A. J. Zolan, and S. Leyffer, "Optimal design and dispatch of a system of diesel generators, photovoltaics and batteries for remote locations," *Optim. Eng.*, vol. 18, no. 3, pp. 755–792, Sep. 2017.
[8] *Homer Pro 3.11 User Manual*, Homer Energy, Boulder, CO, USA, 2017.
[9] J. Sprague, "Optimal scheduling of time-shiftable electric loads in expeditionary power grids," M.S. thesis, Naval Postgraduate School, Monterey, CA, USA, 2015.
[10] S. Bandyopadhyay, T. Ganu, H. Khadilkar, and V. Arya, "Individual and aggregate electrical load forecasting: One for all and all for one," in *Proc. ACM 6th Int. Conf. Future Energy Syst.*, 2015, pp. 121–130.
[11] S. Shabshab, "Fuel-conserving environmental control strategies for small islanded microgrids," M.S. thesis, Dept. Mech. Eng., MIT, Cambridge, MA, USA, Jun. 2018.
[12] M. Gillman *et al.*, "Accounting for every kilowatt," Defense Acquisition Univ., Fort Belvoir, VA, USA, Rep. ADA610754, 2014.
[13] Y. Han, P. Young, and D. Zimmerle, "Constrained optimum generator dispatch for fuel consumption minimization," in *Proc. IEEE Power Energy Soc. Gen. Meeting*, Jul. 2013, pp. 1–5.
[14] S. X. Chen, H. B. Gooi, and M. Q. Wang, "Sizing of energy storage for microgrids," *IEEE Trans. Smart Grid*, vol. 3, no. 1, pp. 142–151, Mar. 2012.
[15] H. Wang, Q. Lv, G. Yang, and H. Geng, "Siting and sizing method of energy storage system of microgrid based on power flow sensitivity analysis," *J. Eng.*, vol. 2017, no. 13, pp. 1974–1978, 2017. [Online]. Available: https://ieeexplore.ieee.org/document/8311091
[16] C. K. Lee, S. C. Tan, F. F. Wu, S. Y. R. Hui, and B. Chudhuri, "Use of Hooke's law for stabilizing future smart grid—The electric spring concept," in *Proc. IEEE Energy Convers. Congr. Expo.*, Sep. 2013, pp. 5253–5257.
[17] T. Logenthiran, D. Srinivasan, and T. Z. Shun, "Demand side management in smart grid using heuristic optimization," *IEEE Trans. Smart Grid*, vol. 3, no. 3, pp. 1244–1252, Sep. 2012.
[18] N. Lu, "An evaluation of the HVAC load potential for providing load balancing service," *IEEE Trans. Smart Grid*, vol. 3, no. 3, pp. 1263–1270, Sep. 2012.
[19] P. Arun, R. Banerjee, and S. Bandyopadhyay, "Optimum sizing of battery-integrated diesel generator for remote electrification through design-space approach," *Energy*, vol. 33, no. 7, pp. 1155–1168, 2008.
[20] E. Hittinger, T. Wiley, J. Kluza, and J. Whitacre, "Evaluating the value of batteries in microgrid electricity systems using an improved energy systems model," *Energy Convers. Manag.*, vol. 89, pp. 458–472, Jan. 2015.
[21] S. A. Pourmousavi and M. H. Nehrir, "Demand response for smart microgrid: Initial results," in *Proc. ISGT*, Jan. 2011, pp. 1–6.
[22] S. A. Pourmousavi and M. H. Nehrir, "Real-time central demand response for primary frequency regulation in microgrids," *IEEE Trans. Smart Grid*, vol. 3, no. 4, pp. 1988–1996, Dec. 2012.
[23] S. Pourmousavi, S. N. Patrick, and M. H. Nehrir, "Real-time demand response through aggregate electric water heaters for load shifting and balancing wind generation," *IEEE Trans. Smart Grid.*, vol. 5, no. 2, pp. 769–778, Mar. 2014.
[24] S. A. Pourmousavi, M. H. Nehrir, and R. K. Sharma, "Multi-timescale power management for islanded microgrids including storage and demand response," *IEEE Trans. Smart Grid*, vol. 6, no. 3, pp. 1185–1195, May 2015.
[25] Z. Xu, R. Diao, S. Lu, J. Lian, and Y. Zhang, "Modeling of electric water heaters for demand response: A baseline PDE model," *IEEE Trans. Smart Grid*, vol. 5, no. 5, pp. 2203–2210, Sep. 2014.
[26] M. Avci, M. Erkoc, A. Rahmani, and S. Asfour, "Model predictive HVAC load control in buildings using real-time electricity pricing," *Energy Build.*, vol. 60, pp. 199–209, May 2013.
[27] S. Lu *et al.*, "Centralized and decentralized control for demand response," in *Proc. ISGT*, 2011, pp. 1–8.
[28] C. Chen, J. Wang, and S. Kishore, "A distributed direct load control approach for large-scale residential demand response," *IEEE Trans. Power Syst.*, vol. 29, no. 5, pp. 2219–2228, Sep. 2014.
[29] C.-M. Chu, T.-L. Jong, and Y.-W. Huang, "A direct load control of air-conditioning loads with thermal comfort control," in *Proc. IEEE Power Eng. Soc. Gen. Meeting*, vol. 1, Jun. 2005, pp. 664–669.

[30] R. Tang, S. Wang, and C. Yan, "A direct load control strategy of centralized air-conditioning systems for building fast demand response to urgent requests of smart grids," *Autom. Construct.*, vol. 87, pp. 74–83, Mar. 2018.
[31] T. Tran-Quoc, J. C. Sabonnadiere, N. Hadjsaid, and C. Kieny, "Air conditioner direct load control in distribution networks," in *Proc. IEEE Bucharest PowerTech*, Jun. 2009, pp. 1–6.
[32] R. Kelly, "Optimizing gas generator efficiency in a forward operating base using an energy management system," M.S. thesis, Naval Postgraduate School, Monterey, CA, USA, 2013.
[33] R. L. Kelly, G. Oriti, and A. L. Julian, "Reducing fuel consumption at a remote military base: Introducing an energy management system," *IEEE Electrific. Mag.*, vol. 1, no. 2, pp. 30–37, Dec. 2013.
[34] J. Olabode, "Analysis of the performance of an optimization model for time-shiftable electrical load scheduling under uncertainty," M.S. thesis, Naval Postgraduate School, Monterey, CA, USA, 2016.
[35] W. Shi, N. Li, X. Xie, C.-C. Chu, and R. Gadh, "Optimal residential demand response in distribution networks," *IEEE J. Sel. Areas Commun.*, vol. 32, no. 7, pp. 1441–1450, Jul. 2014.
[36] W. Zheng, W. Wu, B. Zhang, and C. Lin, "Distributed optimal residential demand response considering operational constraints of unbalanced distribution networks," *IET Gener. Transm. Distrib.*, vol. 12, no. 9, pp. 1970–1979, May 2018.
[37] *Approximate Diesel Fuel Consumption Chart. Diesel Service and Supply*. Accessed: Oct. 8, 2019. [Online]. Available: http://www.dieselserviceandsupply.com/Diesel_Fuel_Consumption.aspx
[38] C. Laughman *et al.*, "Power signature analysis," *IEEE Power Energy Mag.*, vol. 1, no. 2, pp. 56–63, Mar./Apr. 2003.
[39] S. Krishnamoorthy, M. Modera, and C. Harrington, "Efficiency optimization of a variable-capacity/variable-blower-speed residential heat-pump system with ductwork," *Energy Build.*, vol. 150, pp. 294–306, Sep. 2017.
[40] A. T. de Almeida, F. J. T. E. Ferreira, and D. Both, "Technical and economical considerations in the application of variable-speed drives with electric motor systems," *IEEE Trans. Ind. Appl.*, vol. 41, no. 1, pp. 188–199, Jan./Feb. 2005.
[41] N. T. Gayeski, P. R. Armstrong, and L. K. Norford, "Predictive precooling of thermo-active building systems with low-lift chillers," *HVACR Res.*, vol. 18, pp. 858–873, Aug. 2012.

Spencer C. Shabshab received the master's degree in mechanical engineering from the Massachusetts Institute of Technology in 2018. He is a Submarine Officer with U.S. Navy.

Peter A. Lindahl received the B.S. degree in electrical engineering from Pennsylvania State University in 2003, and the M.S. degree in electrical engineering and the Ph.D. degree in engineering from Montana State University in 2009 and 2013, respectively. In 2014, he joined the Research Laboratory of Electronics, Massachusetts Institute of Technology as a Post-Doctoral Associate. He is currently a Senior Associate with the Electrical Engineering and Computer Science Practice, Exponent Inc., where he provides technical consulting services regarding energy and power systems, electromechanical machinery, sensors and instrumentation, and industrial controls.

J. Kendall Nowocin received the Doctoral degree from the Massachusetts Institute of Technology in 2017. He has experience with developing small and large power systems ranging from 10 kW residential and 100 kW industrial electrical projects for Atlantic Electric LLC to a 2.4-GW power plant for a South Carolina power utility. He is currently the CTO and the Co-Founder with CoolCrop, a social entrepreneurship startup in agriculture technology and microgrids.

John Donnal received the B.S. degree in electrical engineering from Princeton University, Princeton, NJ, USA, in 2007, and the M.S. and Ph.D. degrees in electrical engineering from the Massachusetts Institute of Technology, Cambridge, MA, USA, in 2013 and 2016, respectively. He is currently as a Faculty Member with the U.S. Naval Academy in Weapons and Systems Engineering. His research interests include nonintrusive load monitoring synthesis, energy harvesting, and communications systems.

David Blum received the B.A.E. degree from the Department of Architectural Engineering, Pennsylvania State University in 2011, and the M.S. and Ph.D. degrees in building technology from the Massachusetts Institute of Technology in 2013 and 2016, respectively. He is currently a Principal Scientific Engineering Associate with the Building Technology and Urban Systems Division, Lawrence Berkeley National Laboratory. His research focuses on the development and implementation of next-generation computational tools for buildings operating in isolation or within broader energy networks.

Les Norford received the B.S. degree in engineering science from Cornell University, Ithaca, NY, USA, in 1973, and the Ph.D. degree in mechanical and aerospace engineering from Princeton University, Princeton, NJ, USA, in 1984. He is currently a Professor of building technology with the Department of Architecture, Massachusetts Institute of Technology, Cambridge, MA, USA. His research interests include monitoring the performance of mechanical and electrical equipment in buildings, optimization techniques as applied to the design and operation of buildings and their mechanical systems, and measurements and simulations of the interaction of buildings with electricity distribution systems and urban environments.

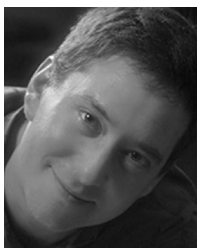

Steven B. Leeb received the Doctoral degree from the Massachusetts Institute of Technology (MIT) in 1993, where he has been a member with the Department of Electrical Engineering and Computer Science since 1993. He also holds a joint appointment with the Department of Mechanical Engineering, MIT. He is concerned with the development of signal processing algorithms for energy and real-time control applications.